Contents lists available at ScienceDirect

Innovative Food Science and Emerging Technologies

Time-dependent model of temperature distribution in continuous flow pulsed electric field treatment chambers

Peter Lombergar , Karel Flisar , Damijan Miklavčič , Samo Mahnič-Kalamiza [*]

University of Ljubljana, Faculty of Electrical Engineering, Tržaška c. 25, SI-1000 Ljubljana, Slovenia

ABSTRACT

A key component of a continuous flow pulsed electric field (PEF) system is the treatment chamber, where the product is exposed to electric pulses. Determination of the temperature distribution in the chamber during PEF treatment is important since high local increases in temperatures can affect the quality of the product. Coupled simulations of electric field, fluid flow, and heating in the existing literature do not model each individual electric pulse, but rather employ a "duty cycle" approach, which does not account for transient variations in treatment intensity and temperature changes in the medium. We present a time-dependent approach to modelling PEF treatment in continuous flow treatment chambers, which can model each pulse separately, and thus enables a more accurate study of temporal and spatial distributions of electric field and temperature. The model has been validated on laboratory scale treatment chambers of parallel plate or colinear design and using realistic protocols.

Industrial relevance text: The paper is relevant to all pulsed electric field (PEF) applications either on laboratory or industrial scale that implement a continuous flow treatment chamber. It presents an improved modelling approach which allows for an analysis of the electrical current, electric field, and temperature distribution in the chamber during, at the end, and in between application of electrical pulses. The model can be used to predict the peak temperature at the end of each pulse in the hot spots, which if large enough could potentially lead to thermal damage of the product or in extreme cases even potential local boiling of the medium, resulting not only in degradation of the treated product, but also in accelerated electrode fouling, oxidation, and dissolution (etching), as well as arcing. This would not only affect the quality of the treated product but would also affect the wear and lifetime of electrodes/chambers, and of the pulse generator. The model can also be used to avoid expensive trial-and-error optimization of the PEF protocols and chamber geometries in situ.

1. Introduction

Exposure of cells to short electrical pulses of sufficiently high amplitude to cause a transient increase in cell membrane permeability is called electroporation (Kotnik, Rems, Tarek, & Miklavčič, 2019). If the exposure of the membrane to an electric field is short enough and not too intense, and the membrane recovers sufficiently rapid for the cell to remain viable, electroporation is termed reversible. The excessive exposure to electric field results in cell death and the electroporation is termed irreversible (Kotnik, Kramar, Pucihar, Miklavcic, & Tarek, 2012). An important feature of electroporation is its universality. It can be achieved in all cell types and in any cell arrangement (Rems & Miklavčič, 2016). Because of this universality, electroporation is now used in various fields: medicine (Geboers et al., 2020; Harris & Elmer,

2021; Sachdev, Potočnik, Rems, & Miklavčič, 2022; Verma, Asivatham, Deneke, Castellvi, & Neal, 2021; Yarmush, Golberg, Serša, Kotnik, & Miklavčič, 2014), biotechnology (Kotnik et al., 2015), environmental applications (Ballash et al., 2020; Golberg et al., 2016), and the food industry (Mahnič-Kalamiza, Vorobiev, & Miklavčič, 2014; Toepfl, Siemer, Saldaña-Navarro, & Heinz, 2014).

In the field of food industry, biotechnology, and environmental engineering, electroporation is often referred to as pulsed electric field (PEF) treatment. One of the most important applications of PEF treatment in the food industry is microbial inactivation through the mechanism of irreversible electroporation (juices (Gabrić et al., 2018), milk (Bermúdez-Aguirre, Dunne, & Barbosa-Cánovas, 2012), wine (Delso, Berzosa, Sanz, Álvarez, & Raso, 2021)). PEF is considered a non-thermal food preservation method, which makes it more attractive than

---

* Corresponding author at: University of Ljubljana, Faculty of Electrical Engineering, Tržaška cesta 25, SI-1000 Ljubljana, Slovenia.
 E-mail address: samo.mahnic-kalamiza@fe.uni-lj.si (S. Mahnič-Kalamiza).

conventional thermal methods because it can better preserve the sensory, nutritional, and functional properties of foods (Gabrić et al., 2018; Mañas & Pagán, 2005; Toepfl, Mathys, Heinz, & Knorr, 2006).

A key component of the PEF treatment system is the treatment chamber, where the product is exposed to electrical pulses. It consists of at least two electrodes and insulating material in between in different geometrical configurations, which result in different electric field distributions in the chamber. We distinguish between static and continuous flow treatment chambers. The former design is primarily intended for laboratory experiments, while continuous flow treatment chambers can more easily be integrated into industrial processes (food industry and biotechnology). In our paper, we focus on the latter (i.e., continuous flow treatment chambers). The most common forms of continuous flow treatment chambers are parallel plate, colinear, and co-axial, with each having their advantages and drawbacks relevant to the PEF processing (Morales-de la Peña, Elez-Martínez, & Martín-Belloso, 2011; Toepfl et al., 2014).

Numerical simulations in the field of PEF treatment can be divided into two groups, according to Gerlach et al. (Gerlach et al., 2008). The first focuses on the simulations of the electric field in different treatment chambers, ignoring fluid flow and heating. The objective of these simulations is to improve the uniformity of the electric field inside the treatment chamber (B. Qin, Zhang, Barbosa-Cánovas, Swanson, & Pedrow, 1995; Góngora-Nieto, Pedrow, Swanson, & Barbosa-Cánovas, 2003; Meneses, Jaeger, Moritz, & Knorr, 2011; Toepfl, Heinz, & Knorr, 2007). The second group of simulation approaches often encountered in the field of PEF treatment focuses on the coupled simulations of the electric field, fluid flow, and heating (Buckow, Schroeder, Berres, Baumann, & Knoerzer, 2010; Buckow, Semrau, Sui, Wan, & Knoerzer, 2012; Fiala, Wouters, van den Bosch, & Creyghton, 2001; Huang, Yu, Gai, & Wang, 2013; Jaeger, Meneses, & Knorr, 2009; Knoerzer, Baumann, & Buckow, 2012; Lindgren, Aronsson, Galt, & Ohlsson, 2002; Schottroff et al., 2020). The focus of these simulations is to study and understand the potential interplay of resistive (ohmic) heating of the product due to electric current and heat transfer through convection and conduction.

Determination of the temperature distribution in a treatment chamber during PEF treatment is important since the local temperature variations inside the chamber due to an inhomogeneous electric field distribution and fluid velocity profile can affect the quality of the product during treatment as not all trajectories are equivalent in terms of exposure. If the temperature rise is large enough, PEF technology may risk losing the advantage of its non-thermal nature.

The aforementioned coupled simulations of continuous flow PEF treatment chambers in the existing literature do not model temporally variable electric fields, but instead use a time-invariant potential as a boundary condition. To model the temperature increase, the steady state ohmic heating source (Q_{ec}) is multiplied by a duty factor (τf) to relate it to the pulsating heating source, where τ represents the pulse width and f the pulse repetition frequency.

$$Q = \tau f \cdot Q_{ec} = \tau f \cdot \sigma E^2 \quad (1)$$

While this "duty cycle" approach to modelling the time-dependent electric field and heating reduces computational complexity, it comes with potential drawbacks. In the duty cycle approach, ohmic heating is assumed to occur only during the duration τ of a perfectly square-shaped pulse with a negligible rise and fall time. Since the pulses are not always perfectly square-shaped, especially at lower pulse widths, this approach may not accurately describe the heating in the treatment chamber. The duty cycle approach also does not give us a complete picture of the temperature changes during each individual electrical pulse, i.e., we miss the peak temperature at the end of the pulse and decrease in temperature between the pulses. In this respect, our study differs from studies reported on in existing literature, as it departs from the duty cycle approach.

To describe the temperature distribution in the treatment chamber as accurately as possible, we developed and present a time-dependent approach to modelling the electric field and heating. The goal was to first build a coupled multiphysics model of a PEF treatment chamber, which can model each pulse separately, and then validate it for different treatment chambers and pulse protocols. To the best of our knowledge, such an approach (i.e., time-dependent) has not been utilized or reported on before in the literature in the context of multiphysics modelling of electric field, fluid flow, and heating.

2. Materials and methods

The complete experimental setup is shown in Fig. 1. For experiments, 0.18% NaCl$_{(aq)}$ solution was chosen, since its electrical conductivity closely resembles the electrical conductivity of fruit juices, in particular that of fresh orange juice. Conductivity of 0.18% NaCl$_{(aq)}$ at 25 °C calculated with the model described in (McCleskey, 2011) is 0.352 S/m, and the mean value of fresh natural orange juice at 25 °C is 0.343 S/m according to (Prasad Lamsal & Kumar Jindal, 2014), therefore, the 0.18% saline solution can be considered a good electrical model of freshly squeezed orange juice. We obtained 0.18% saline by diluting a commercial 0.9% NaCl$_{(aq)}$ solution (B. Braun, Melsungen, Germany) with a topical irrigation solution (Aqua by B. Braun, Melsungen, Germany), in a 1:4 ratio.

Saline solution was pumped with a syringe pump Aladin-1000 (World Precision Instruments, USA) and commercial 50 ml plastic syringe (BD Plastipak). Aladin-1000 syringe pump allows for a maximum syringe volume up to 60 ml and a maximum pumping rate of 35.3 ml/min.

Two different continuous flow treatment chambers were used in experiments. A colinear treatment chamber (Eleršek et al., 2020), and a parallel plate treatment chamber (Pataro, Ferrentino, Ricciardi, & Ferrari, 2010), both kindly provided to us by Gianpiero Pataro (University of Salerno, Fisciano, Italy), hereon referred to as the *colinear* and the *parallel plate* treatment chambers, respectively (Fig. 2).

During the experiments, the treatment chambers were set up vertically with the saline solution pumped against gravity to allow the gas bubbles potentially being formed on the electrodes during the application of the pulses to exit the chamber.

Masterflex 96,410–16 silicone tubes with internal diameter of 3.1 mm (Cole-Parmer, USA) were used to connect the syringe pump to inlet and outlet of the parallel plate treatment chamber to a waste reservoir.
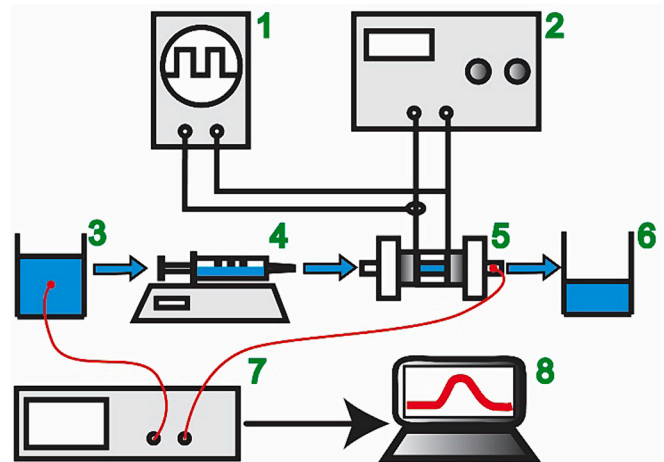

Fig. 1. Schematic representation of the experimental setup: oscilloscope (1) and pulse generator (2); middle row: 0.18% NaCl$_{(aq)}$ solution (3), syringe pump (4), continuous flow treatment chamber (5), and waste reservoir (6); bottom row: optical thermometer (7) with temperature sensors in red, and computer (8). (For interpretation of the references to colour in this figure legend, the reader is referred to the web version of this article.)
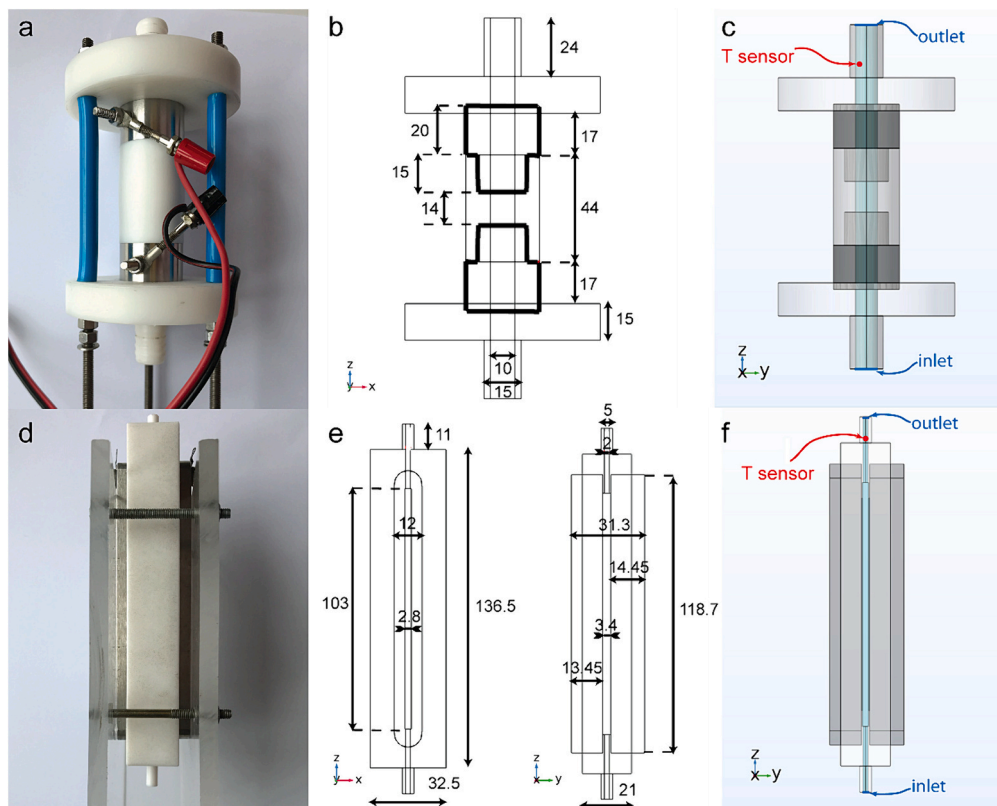
Fig. 2. Continuous flow treatment chambers used in experiments and in the numerical model; a) a photo of the colinear treatment chamber, b) a detailed geometry of the colinear treatment chamber with measurements (in mm), c) a 3-D geometry of the colinear treatment chamber used in the numerical model (electrodes are colored in gray), d) a photo of the parallel plate treatment chamber, e) a detailed geometry of the parallel plate treatment chamber with measurements (in mm), f) 3-D geometry of the colinear treatment chamber used in the numerical model (electrodes are colored in gray). Red dots in c) and f) represent the approximate temperature sensor position during the experiments. (For interpretation of the references to colour in this figure legend, the reader is referred to the web version of this article.)

In case of the colinear treatment chamber, silicone tubes from a local manufacturer with a 12 mm internal diameter were used.

A new plastic syringe was used for each experiment and prior to and after each experiment, silicone tubes were flushed with distilled water. After each experiment, continuous flow treatment chambers were cleaned by distilled water and disassembled prior to each experiment to polish the electrodes and thoroughly clean them with 70% ethanol, after which they were rinsed with distilled water before reassembly.

Unipolar square wave pulses were applied using a pulse generator designed and described previously in (Flisar, Meglic, Morelj, Golob, & Miklavcic, 2014). To generate square-shaped pulses, pulse generator "Bruno" uses a high voltage switch, made of series-connected optically-driven transistors. Maximum output voltage of the pulse generator is 5000 V and the maximum output current 100 A, possible pulse lengths are 10 μs, 50 μs, 100 μs, 500 μs, 1 ms, 5 ms, and 10 ms, with pulse repetition frequencies of 1 Hz, 10 Hz, and 100 Hz, and an option of manually choosing a discrete number of pulses to be applied (between 1 and 99), or operating in continuous pulse delivery mode.

Voltage and current were recorded in sequential capture mode with a Digital Signal Oscilloscope LeCroy HDO6104A-MS (Teledyne LeCroy, USA) using a 100 MHz high-voltage differential probe (LeCroy HVD3605A), and a 100 MHz current probe (LeCroy CP031A).

During each pulse protocol application, the temperature at the outlet of the chamber was recorded using the OpSens optical thermometer PSC-D-N-N equipped with 4 single-channel modules of type PSR-G1–10-100ST (OpSens Solutions INC, Canada) and an OpSens OTG-MPK5 fibreoptic temperature sensor. The optic sensor used has a response time lower than 225 ms and high accuracy of ±0.3 °C across its operating range of 20 to 150 °C. Signals recorded were processed with OpSens software SoftProSense, where a running average filter with kernel size of 10 was applied to all measurements for improving the signal-to-noise ratio. The sensor was positioned at the outlet at the location marked in Fig. 2c and f. The temperature of both the 0.18% NaCl solution used for experiments and the environment (room temperature) were being monitored for reference.

Electrical conductivity of the NaCl solution was measured/controlled using the conductometer SevenCompact (MetlerToledo, USA) before performing the experiments.

2.1. Treatment chambers

Fig. 2 shows the colinear and the parallel plate treatment chamber used in experiments, together with detailed geometries and measurements, which were used to produce the 3-D geometries in the numerical model.

Colinear treatment chamber is made of a Teflon holder and two stainless steel electrodes with the inter electrode distance (L) of 14 mm (decreased from 15 mm originally, likely a consequence of material degradation due to frequent use of the treatment chamber), with an inner diameter of 10 mm, which results in a treatment volume (active part of the chamber) of 1.1 ml.

Parallel-plate treatment chamber was originally made of a Teflon holder and two stainless steel electrodes with initial inter electrode distance of 2.5 mm and width and length of the treatment volume being 2.8 mm and 103 mm, respectively. However, due to leakage of fluid (likely due to numerous assembly/disassembly cycles), it was slightly modified for the purposes of conducting our experiments. Silicone rubber gaskets were added between electrodes and the whole chamber was

compressed between two sheets of acrylic glass. With addition of silicone gaskets, the new inter-electrode distance (L) was 3.4 mm and the surface area of electrodes was decreased from 288 mm^2 to 219 mm^2, since compression of the gaskets caused them to extend laterally and partially obstruct the electrode-fluid boundary surface. This was all accounted for in the numerical model and it resulted in irregularly shaped treatment volume of 0.826 ml (further elaborated in the Supplements section, Fig. S1).

2.2. Pulse protocols

Two different pulse application modes were used: fixed number of pulses and continuous pulse delivery. We focused on a fixed number of pulses for easier numerical simulations and evaluation of the results. However, in practical use of continuous flow treatment chambers, evaluating continuous pulse application is critical. For this reason, we incorporated two continuous pulse application protocols for each treatment chamber in our study, where we focused on achieving stationary conditions (i.e., steady state outlet temperature) in the experiments and in the model.

Pulse protocols used in this study are given in Table 1 together with key PEF parameters according to (Raso et al., 2016). An example of the pulse shape can be seen in Fig. 3.

Pulses trains are listed as:

$$N \times \tau, f \tag{2}$$

Where N represents number total number of pulses. In case of continuous pulse application, abbreviation *cont.* is used. The variable τ represents pulse width, which for a square pulse is t_{FWHM} - full width of the pulse at half maximum value (Rebersek, Miklavcic, Bertacchini, & Sack, 2014). Pulse repetition frequency is represented as f. Volumetric flow rates (F) were chosen with regards to treatment volume (v) and limitations of the used syringe pump Alladin-1000. Peak voltage (U) was chosen within the limitations of the pulse generator, the high-voltage probe, and the current probe, so as to avoid dielectric breakdowns (sparking or arcing) and damage to the voltage/current probes. For better comparability of results across experiments and different studies, it is useful to define the "voltage-to-distance" ratio or *VDR* as the peak voltage (U) divided by the inter-electrode distance L (Eq. (3)).

$$VDR = \frac{U}{L} \tag{3}$$

The *VDR* can be considered a good estimation of the electric field strength in the treatment volume in the case of parallel plate electrode
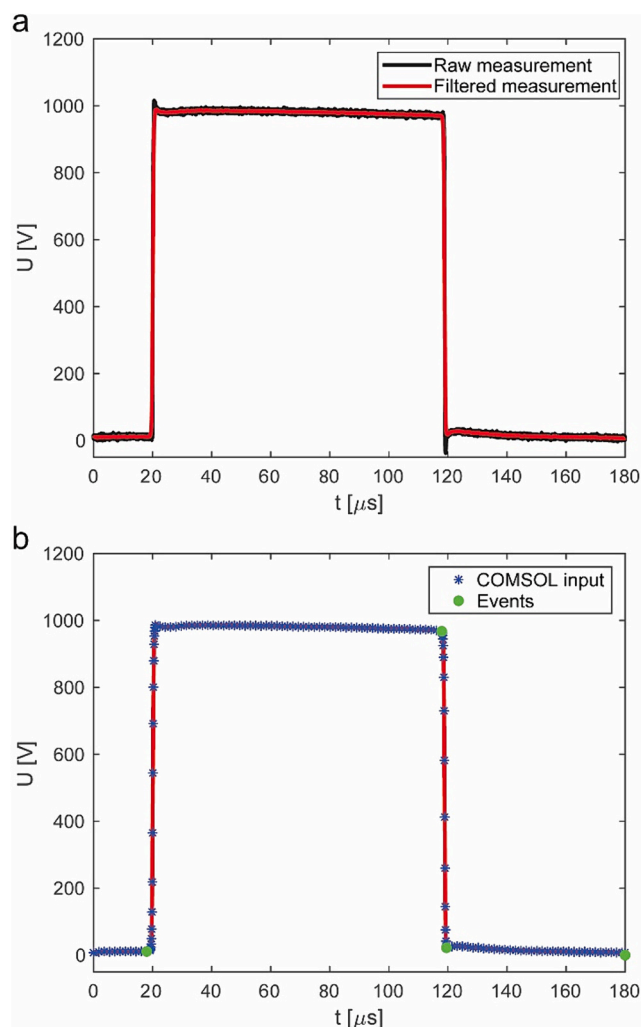

Fig. 3. Representative unipolar square wave pulses as applied and measured in experiments and used in the model. (a) Recorded voltage signal for a representative pulse from the 10 × 100 μs pulse protocol for the parallel plate treatment chamber, and the corresponding filtered and decimated signal. (b) Individual pulse points (blue asterisks) imported into the numerical model, with event points (green dots) used to accurately model the time varying voltage. (For interpretation of the references to colour in this figure legend, the reader is referred to the web version of this article.)

configuration and not in the case of colinear electrode configuration due to non-uniform distribution of electric field. To more accurately estimate the electric field in the treatment volume we can use results from numerical simulations (Fig. S2 and S3).

In continuous pulse application mode, the number of pulses applied n is not directly set by the user as in the batch treatment, but rather as a function of pulse frequency (f) and residence time t_r of the product in the treatment chamber, which depends on the flow rate (F) and treatment volume of the chamber (v). The number of pulses can be calculated according to Eq. (4).

$$n = t_r \cdot f = \frac{v}{F} \cdot f \tag{4}$$

Treatment time is defined as number of applied pulses, multiplied by the pulse width (Eq. (5)).

$$t = n \cdot \tau \tag{5}$$

W_T represents total specific energy input and can be calculated by multiplying the specific energy per pulse W by the number of pulses applied n (Eq. (7)). W represents electrical energy received by the

Table 1
Pulse protocols and key PEF parameters.

Treatment chamber	Pulse protocol (2)	F [ml/min]	U [V]	VDR [V/cm]	n	t [μs]	W_T [kJ/kg]
Colinear	10 × 100 μs, 1 Hz	10	4000	2860	6.6	660	15.6
		20			3.3	330	7.8
	cont. 100 μs, 1 Hz	20			3.3	330	7.8
	64 × 10 μs, 10 Hz	10			64*	640*	15.1*
		20			33	330	7.8
	cont. 10 μs, 10 Hz	20			33	330	7.8
Parallel Plate	10 × 100 μs, 1 Hz	10	1000	2940	5	500	14.0
		20			2.5	250	7.0
	cont. 100 μs, 1 Hz	20			2.5	250	7.0
	64 × 10 μs, 10 Hz	10			50	500	14.0
		20			25	250	7.0
	cont. 10 μs, 10 Hz	20			25	250	7.0

* N < n, total number of pulses (N) is smaller than calculated number of pulses applied (n).

treated product per each pulse and is evaluated by integrating the recorded current and voltage waveforms over time for a single representative pulse (Eq. (6)).

$$W = \frac{1}{m} \int_0^\infty U(t) \cdot I(t) dt = \frac{1}{v^* \rho_{H_2O}} \int_0^\infty U(t) \cdot I(t) dt \qquad (6)$$

$$W_T = W \cdot n \qquad (7)$$

Here it is important to mention that the residence time (t_r), with which we calculate the number of pulses applied (Eq. (4)), represents the average residence time of the product in the treatment volume (active part of the chamber). This means that number of pulses applied, treatment time, and total specific energy all represent average values received by the product. Depending on the trajectory of the product in the treatment chamber and the flow velocity profile these values can vary, i.e., in the case of the parabolic velocity profile, the residence time of the product flowing along the walls of the treatment volume is longer than for the product flowing in the middle of the channel.

2.3. Numerical model

COMSOL Multyphysics (Version 6.0, COMSOL AB, Sweden) was used for numerical modelling. First, the accurate 3-D geometries were created for both treatment chambers (Fig. 2c and f).

To accurately model the temperature distribution in the treatment chamber as a result of ohmic heating and heat transfer by advection and conduction, the following COMSOL interfaces were used: Laminar Flow, Electric Currents, Heat Transfer in Solids and Fluids, Electromagnetic Heating, and Events.

The workflow of the simulations was as follows: first, the fluid flow through the chamber was solved in a stationary study; the solution from the flow study was then used in the subsequent coupled time-dependent study (one-way coupled), in which the electric field and temperature distribution were solved simultaneously (bidirectionally coupled).

To solve the stationary study, fully coupled solver with automatic damped Newton method was used and to solve the coupled time-dependent study fully coupled solver with constant damped Newton method was used. In the time-dependent study, timesteps of 1/100 of the pulse period ($t_p = f^{-1}$) were specified as output times and the intermediate timestep method was chosen in the solver. This method forces the time-dependent solver to take at least one timestep in each subinterval of the requested output times.

Finite element mesh was built mostly of tetrahedral elements. For boundary layers along the flow channel, prism elements were used and in the case of the parallel plate treatment chamber pyramid elements were used as well to transition between tetrahedrons and prisms. The final mesh was chosen based on the necessary resolution of temperature change in hot spots and simulation time and consisted of 22,110 elements (17,286 tetrahedrons, 4824 prisms) in case of colinear treatment chamber and 139,510 elements (116,318 tetrahedrons, 19,828 prisms, and 3363 pyramids) in case of parallel plate treatment chamber, mesh independence study is shown in the Supplements (Fig. S4).

Numerical simulations were run on the computer with two Intel(R) Xeon(R) Gold 6226R CPU @ 2.90 GHz processors and 384 GB RAM. Simulation times for the continuous pulse protocols in colinear treatment chamber were: 10 h for the 100 μs, 1 Hz protocol (1000 simulated pulses); and 13 h 30 min for the 10 μs, 10 Hz protocol (1400 simulated pulses). Simulations times for the continuous pulse protocols in parallel plate treatment chamber were: 3 h for the 100 μs, 1 Hz protocol (60 simulated pulses); and 9 h 30 min for the 10 μs, 10 Hz protocol (200 simulated pulses).

2.3.1. Fluid flow

Fluid flow through the treatment chamber was assumed to be laminar (Reynolds numbers for colinear and parallel plate treatment chamber and 20 ml/min flow are 42 and 212, respectively) and

incompressible. To model the fluid flow, Laminar flow interface was used in COMSOL, where the incompressible form of the continuity equation (Eq. (8)) for conservation of mass and the Navier–Stokes equation (Eq. (9)) for conservation of momentum were solved for:

$$\nabla (\rho \boldsymbol{u}) = 0 \qquad (8)$$

$$\rho \left(\frac{\partial \boldsymbol{u}}{\partial t} + \boldsymbol{u} \cdot \nabla \boldsymbol{u} \right) = -\nabla p + \nabla \cdot \left(\mu \left(\nabla \boldsymbol{u} + (\nabla \boldsymbol{u})^T \right) \right) \qquad (9)$$

$\boldsymbol{u}$ is the fluid velocity field, p is the fluid pressure, ρ is the fluid density, and μ is the fluid dynamic viscosity. Fluid density was evaluated at the reference pressure of 101.3 kPa and the reference temperature of 20 °C.

Volumetric flow rate was specified as a boundary condition at the inlet and a fully developed flow option was chosen in COMSOL which forces the flow at the inlet toward the solution for a fully developed channel flow (parabolic velocity profile). At the outlet a zero-pressure boundary condition was fixed and at the inner walls of the flow channel, a non-slip boundary condition (i.e., the velocity is set to zero) was specified. Position of the inlet and outlet boundary condition within the geometry of each chamber can be observed in Fig. 2c and f.

2.3.2. Electric field

To model the electric field in the chamber during the pulse delivery, Electric Currents interface was used in COMSOL, where the continuity equation for conservation of charge (Eq. (10)) was solved for time-varying electric fields:

$$\nabla \cdot \boldsymbol{J} + \frac{\partial \rho_e}{\partial t} = 0 \qquad (10)$$

here $\boldsymbol{J}$ is the current density vector and ρ_e is the space charge density.

Electric potential boundary condition was applied at the electrodes. Voltage at the ground electrode was set to zero and at the active electrode, a time-dependent voltage/potential was specified. At all other boundaries around the flow channel including inlet and outlet, electric insulation (i.e., no electric current flows through the boundary) was specified as boundary condition.

To model the electrical pulses of different protocols used in this study as accurately as possible, the voltage recorded by the oscilloscope was used in the model. For each pulse protocol and treatment chamber, a representative pulse was chosen from the voltage recording and was first filtered with a Butterworth filter, then suitably decimated using MAT-LAB (Mathworks, USA) and imported into COMSOL (Fig. 3). The imported waveform served as a basis for an analytical function with a periodic extension, where pulse period ($t_p = f^{-1}$) was specified for each protocol in order to transform the representative pulse into a pulse protocol comprising multiple pulses. The analytical function describing the time-varying voltage for a specified pulse protocol was then used as a boundary condition for the active electrode.

For the COMSOL time-dependent solver to accurately model each square wave electrical pulse, the Events interface was used, which forces the solver to take additional time steps and reinitialize the dependent variables at the specified time of the event. To accurately describe pulses used in our study, four event points with period of event equal to pulse period (t_p), were specified at the critical points of the representative square-shaped pulse (green dots in Fig. 3b). In case of an idealized square-shaped pulse, only two event points are needed: first point at the start of the rising edge of the pulse, and second point at the start of the falling edge of the pulse.

Events presents an efficient and accurate way of modelling the transient behaviour of the solution of the partial deferential equation (e. g. electric potential for charge conservation equation and temperature for the heat transfer equation), when the solution/dependent variable (e.g. electric potential – charge conservation equation) or the load/ source term (e.g. ohmic heating – heat transfer equation) changes on a

time scale that is considerably smaller than the time scale of the whole simulation, without the need to significantly reduce the size of the time steps that the solver takes and thus significantly extend the simulation time.

2.3.3. Temperature field

To model temperature in the treatment chamber, Heat Transfer in Solids and Fluids interface was used in COMSOL, where the heat equation for conservation of energy (Eq. (11)) was solved:

$$\rho c_P \left(\frac{\partial T}{\partial t} + \boldsymbol{u} \cdot \nabla T \right) - \nabla \cdot (k \nabla T) - Q = 0 \quad (11)$$

here ρ is the density, c_P the heat capacity at constant pressure, k is the thermal conductivity, $\boldsymbol{u}$ is the fluid velocity field and Q is the heat source (load). In order to account for ohmic heating, the heat equation was coupled with the electric field. This coupling was done using the Electromagnetic Heating multiphysics coupling interface in COMSOL, which adds an ohmic heating source to the heat equation. In our model, time-dependant (ohmic) heating source was used:

$$Q(t) = Q_{ec}(t) = \sigma(T)E(t)^2 \quad (12)$$

$\sigma(T)$ is the temperature dependent electric conductivity of the fluid/NaCl solution and $E(t)$ is the time-varying electric field distribution in the treatment chamber, which was calculated together with temperature distribution in a coupled time-dependent study. For the convection part of the heat equation, solution from the previous fluid flow study was used as the fluid velocity field.

At the inlet, inflow boundary condition was chosen in COMSOL and upstream temperature was specified. At the outlet, outflow boundary condition was chosen in COMSOL, which imposes a zero gradient in the normal direction. Position of the inflow and outflow boundary conditions are the same as the inlet and outlet boundary conditions for the fluid flow (Fig. 2c and f). On the outer surface of the treatment chamber, thermal insulation boundary condition was used (no heat flux across the boundary), since there is negligible contribution of natural convection to heat dissipation from the treatment chamber surface. For the initial temperature of the treatment chamber and the upstream temperature, temperature of the fluid measured within the outlet of the treatment chamber just before pulse application was specified (T_i).

2.4. Materials

Material properties at room temperature (20 °C) for the treatment chamber and the fluid (saline solution) can be found in Table 2 and Table 3 respectively.

The temperature-dependent material properties for the Teflon holder/insulator (Fig. 2 c and f, white) and stainless-steel electrodes (Fig. 2 c and f, gray) and the 0.18% saline solution were taken from the COMSOL Material Library using materials Teflon (polytetrafluoroethylene), 2101 duplex stainless steel and water respectively. For the 0.18% saline solution, temperature-dependent electrical conductivity was calculated with the model described in (McCleskey, 2011). The calculated temperature-dependent electrical conductivity is given in the supplements (Fig. S5) for reference. The validity of the temperature-dependent electrical conductivity model was checked for the 0.18% saline solution at room temperatures (20–23 °C) and at higher temperatures (60–70 °C) using a conductometer, and the deviation of the model from the measurements was found to be <1%.

Table 2
Material properties at room temperature (20 °C) for the treatment chambers.

Element/Material	k [W/mK]	c_P [J/kgK]	ρ [kg/m³]
Electrodes/Stainless steel	14	500	7760
Insulator/Teflon	0.27	2150	2150

Table 3
Material properties at room (and inlet) temperature (20 °C) for the fluid (saline solution).

Element/Material	k [W/mK]	c_P [J/kgK]	ρ [kg/m³]	σ [S/m]	μ [kg/ms]
Fluid/0.18% NaCl$_{(aq)}$*	0.594	4187	998	0.316	0.001

* Water with modified electrical conductivity.

3. Results and discussion

3.1. Validation of the model

The model was validated against experimentally measured electrical current and temperature of the fluid within the outlet channel of the treatment chambers during pulse application.

Fig. 4 presents the measured and simulated change of temperature within the outlet of colinear and parallel plate treatment chambers for different pulse protocols. Temperature in the simulation was evaluated at the approximate position of the temperature sensor (within the outlet of each treatment chamber) during the experiment (Fig. 2, red dot). Measured temperature data was first filtered with a Butterworth filter, and then the initial temperature of the solution (T_i), before pulse application, was determined from the filtered measurements (Fig. S6). Initial temperature of the solution was used as the initial value of the temperature in the simulation, as well as the inflow temperature (Section 2.3.3). For model validation, so determined initial temperature was subtracted from the measured and simulated values.

A good correlation between simulated and measured values can be observed in Fig. 4 for all pulse protocols in both treatment chambers. In the case of the parallel plate treatment chamber and 100 µs pulses with 1 Hz pulse repetition frequency (Fig. 4a & 4e), we observe temperature oscillations in both measured and simulated temperature, corresponding to pulse repetition frequency (f). These oscillations result from heating of the fluid during pulse duration and consequent increase in temperature, followed by the temperature decrease between the pulses due to convection and conduction. The agreement between the simulated and measured temperature oscillations, shows the ability of the model to accurately predict transient temperature variations during and in between application of electrical pulses.

In the case of the colinear treatment chamber and 100 µs pulses (Fig. 4b & 4f), these oscillations are not visible within the outlet, due to considerable distance of the outlet/temperature sensor from the treatment volume of the chamber. However, the model shows that temperature oscillations are present in the treatment volume (Fig. 6) and could be observed if one would measure the fluid temperature inside the treatment volume.

In continuous pulse application the stationary state was achieved only in the case of the parallel plate treatment chamber (Fig. 4e). In the case of the colinear chamber (Fig. 4f), the syringe volume was not large enough to run the experiment for sufficiently long, which is why the stationary state for the collinear chamber was reached only in the simulation. Overall, good agreement between measured and simulated temperature change within the outlet of both chambers can be observed. Average root mean square error (RMSE) between the model and measurements is 0.05 °C, and the maximum absolute error is 0.24 °C, which is below the accuracy of the temperature sensors used (± 0.3 °C). See Table 4 for RMSE and maximum error for each protocol.

Fig. 5 shows measured and simulated current for the parallel plate (left column), and the colinear (right column) treatment chamber for a representative 10 µs and 100 µs pulse.

In the case of the parallel plate treatment chamber, we can observe a good agreement between the shapes of the measured and the simulated current for both 10 and 100 µs pulse duration (Fig. 5a & 5c). Amplitude of the simulated current is slightly higher than that of the measured current. This could be due to underestimation of the effective electrode
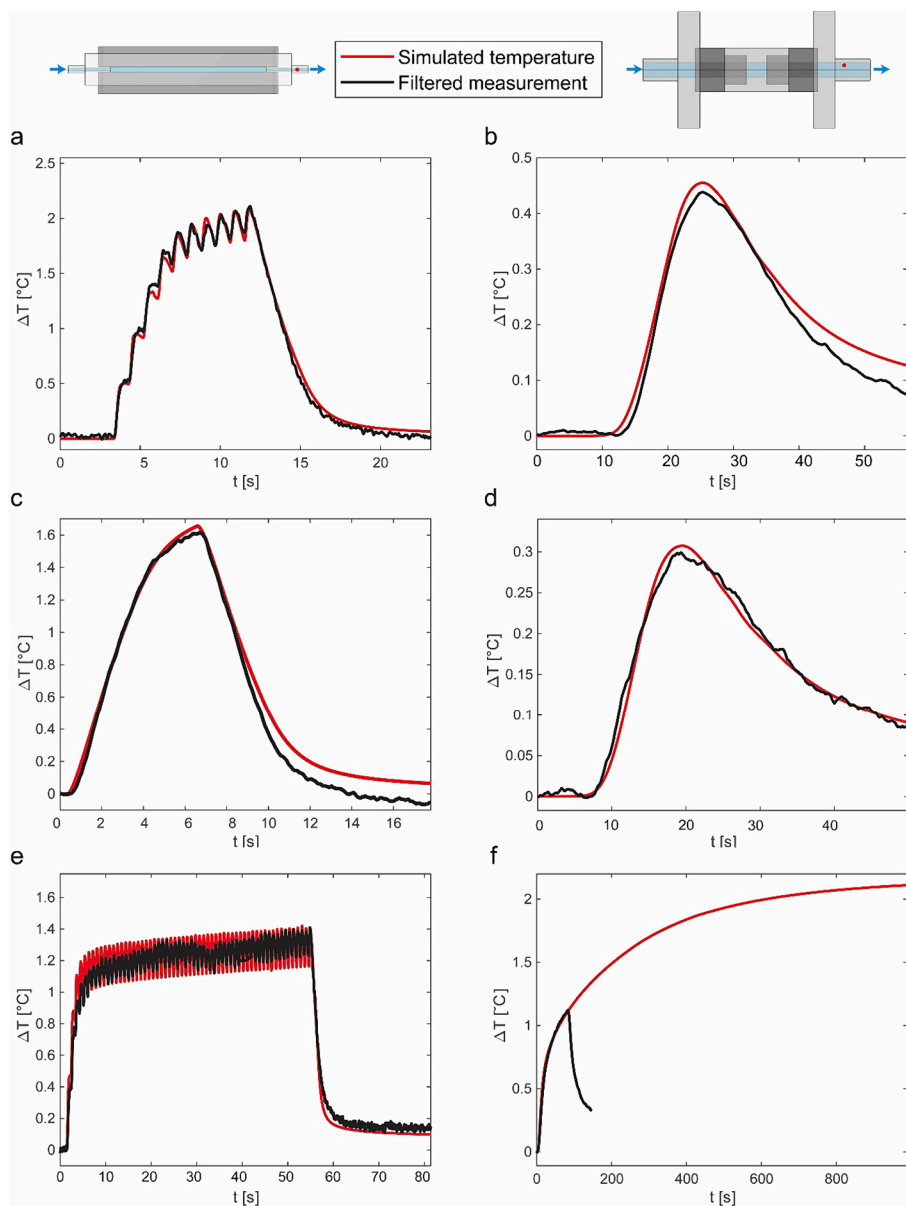
Fig. 4. Comparison of simulated and measured temperature change within the outlet of the parallel plate (left column) and the colinear (right column) treatment chamber during pulse application for different PEF protocols: (a, b) 10 × 100 μs, 1 Hz and F = 10 ml/ min, (c, d) 64 × 10 μs, 10 Hz and F = 10 ml/ min, and (e, f) cont. 100 μs, 1 Hz and F = 20 ml/ min. Voltages used were U = 1000 V for parallel plate chamber (left column), and U = 4000 V for the colinear chamber (right column). Note the different ranges on the *x* and *y* axes.

surface area, i.e., an overestimation of the area of electrodes obstructed by gaskets (Fig. S1). The calculated RMSE between simulated and measured current for the parallel plate chamber is 0.8 A for the 100 μs pulse, and 0.7 A for the 10 μs pulse.

In the case of the colinear chamber, there is a good agreement between the amplitude of the measured and simulated current for both the 10 μs and 100 μs pulses (Fig. 5b & 5d). However, there is a difference in current shape, i.e., the measured current for the colinear chamber shows a current peak that is not present in the simulated current, since the numerical model does not account for the capacitive current. Regarding the difference in the current peak (or lack thereof in the case of the parallel plate chamber) between the two types of chambers (contrast Fig. 5a with b), it should be noted that the estimated capacitance of the parallel plate chamber is higher than the capacitance of the colinear chamber. We would thus expect to see a larger capacitive current peak in the case of the parallel plate chamber. However, there are many factors influencing the capacitive current and its amplitude. First, the capacitive

current equals the derivative of voltage change on time, multiplied by the capacitance of the chamber. In our case the rise time for the parallel plate chamber is almost twice as long as the corresponding rise time for the colinear chamber. Also, the voltage amplitude is four times higher in the colinear chamber. This means the derivative of voltage change during rise time is considerably higher in the case of the colinear treatment chamber. And secondly, the resistive current amplitude is about four times lower in the case of the colinear chamber, and thus the capacitive current contribution is more pronounced for the colinear chamber compared to the parallel plate one, where it is practically absent.

An interesting detail that we can observe in the case of the colinear chamber and the 100 μs pulse (Fig. 5b) is a small increase in the current over the duration of the pulse, which is due to the heating of the treatment volume and thus the increase in the electrical conductivity of the saline and a consequent decrease in the electrical resistance of the chamber.

Table 4
Average root mean square error (RMSE) and maximum absolute error between the calculations from the model and the measurements.

Treatment chamber	Pulses applied (1)	F [ml/min]	U [V]	RMSE [°C]	Max abs error [°C]
Colinear	10 × 100 μs, 1 Hz	10	4000	0.026	0.0521
		20		0.0132	0.0234
	cont. 100 μs, 1 Hz	20		0.0286	0.0662
	64 × 10 μs, 10 Hz	10		0.0093	0.0325
		20		0.0168	0.0415
	cont. 10 μs, 10 Hz	20		0.1433	0.2414
Parallel Plate	10 × 100 μs, 1 Hz	10	1000	0.0460	0.1287
		20		0.0475	0.1629
	cont. 100 μs, 1 Hz	20		0.0601	0.2385
	64 × 10 μs, 10 Hz	10		0.08	0.1395
		20		0.0285	0.0567
	cont. 10 μs, 10 Hz	20		0.0797	0.1724

The calculated RMSE between simulated and measured current for the colinear chamber is 0.4 A for the 100 μs pulse and 0.9 A for the 10 μs pulse.

The numerical model was successfully validated against the experiments by comparing simulated and measured temperature of the fluid within the outlet channel of the treatment chambers and simulated and measured electrical current. The model reliably predicted the amplitude and the temporal dynamics of both temperature rise and electrical current during pulse application for both treatment chambers and across different treatment protocols used in the experiments. Overall, these results provide confidence in the model developed and its ability to predict temperature and electric field distribution in the treatment chamber during pulse application independent of the pulse protocol, flow parameters, and treatment chamber design.

3.2. Temperature distribution

Fig. 6 shows the simulated temperature distribution in the colinear treatment chamber for the 100 μs, 1 Hz continuous pulse application protocol. In Fig. 6a, we can observe the spatial temperature distribution in the treatment chamber at the end of the last pulse. Notably, the highest temperature rise is predicted at the end of the treatment volume near the electrode edge. This hot spot is caused by the high energy received by the saline flowing through the specified location. Due to the parabolic flow velocity profile, the product (saline in our case) flowing near the channel walls receives a higher number of pulses and thus energy than the product flowing in the centre of the channel, when passing through the treatment volume. As a result, the largest temperature rise is observed for the saline flowing near the channel walls upon exiting the treatment volume. Moreover, the high electric field strength and current density around the electrode edges add to the received energy load and consequently temperature rise in this region. In Fig. 6b, temperature change during pulse application is evaluated at three different locations in the treatment chamber (visible in Fig. 6a): i) at the hot spot at the end of the treatment volume near the electrode edge; ii) exactly in the middle of the treatment volume; and iii) at the outlet of the treatment chamber. As expected, the temperature rise at the hot spot is much greater than the temperature rise in the middle of the treatment volume. The model also predicts temperature oscillations at the hot spot and in the middle of the chamber, corresponding to the pulse repetition frequency (f). These temperature oscillations are, however, not present
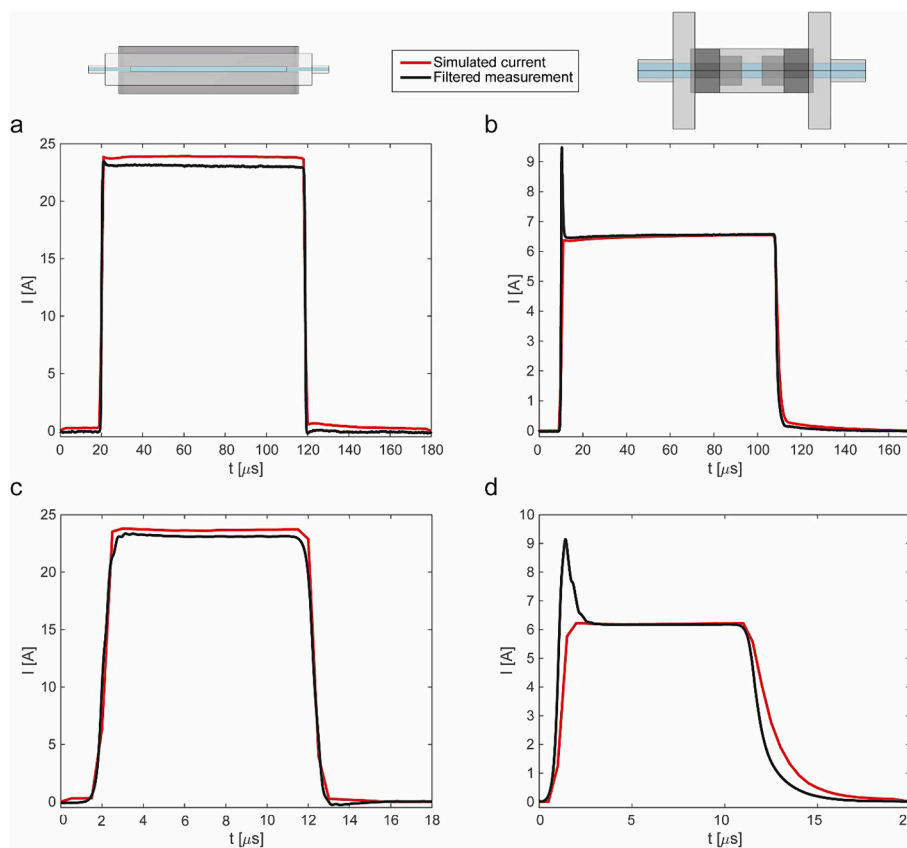

Fig. 5. Comparison of simulated and measured electrical current for parallel plate (left column) and colinear (right column) treatment chamber for a representative pulse from different PEF protocols: (a, b) 10 × 100 μs, 1 Hz and F = 10 ml/min, and (c, d) 64 × 10 μs, 10 Hz and F = 10 ml/min. Voltages used were U = 1000 V for parallel plate chamber (left column) and U = 4000 V for the colinear chamber (right column). Note the different ranges on the x and y axis.
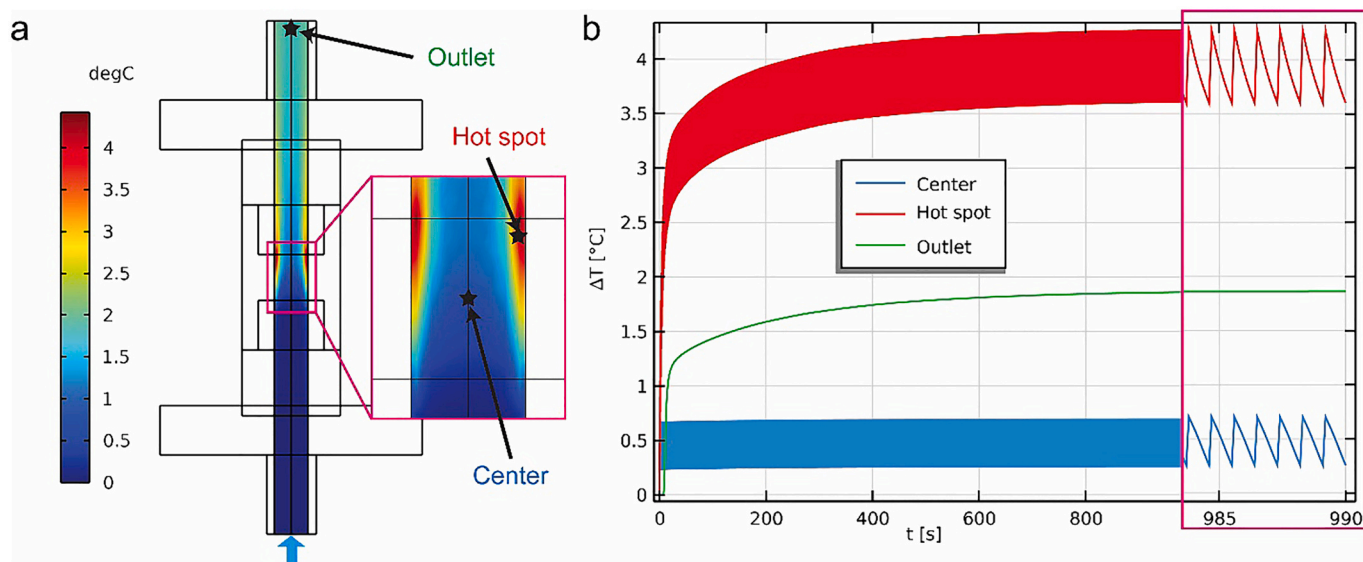
Fig. 6. (a) Simulated temperature distribution along the longitudinal symmetry plane of the co-linear treatment chamber at the end of last simulated pulse for pulse protocol: continuous 100 μs, 1 Hz, U = 4000 V and F = 20 ml/min. (b) Temperature change evaluated at three different locations in the chamber (Hot spot, Outlet, Center - visible in (a)), for the same pulse protocol.

at the outlet of the treatment chamber where temperature was measured because the outlet is further away from the treatment volume where the ohmic heating takes place and the channel through which the fluid flows acts as a low-pass filter.

Fig. 7 shows the simulated temperature distribution in the parallel plate treatment chamber for the 100 μs, 1 Hz continuous pulse application protocol. Similarly, as in the case of the colinear treatment chamber, the highest temperature rise is predicted at the end of the treatment volume near the electrode edge (Fig. 7a). However, the

differences in temperature rise in different locations inside the treatment chamber are smaller, compared to the colinear treatment chamber. More homogeneous spatial temperature distribution in the treatment volume of the parallel plate treatment chamber compared to the colinear can be attributed to a more homogeneous electric field distribution. Expectedly, we can also observe temperature oscillations at all three (evaluated) locations in the chamber, including the outlet (proven by experiments), since the outlet is closer to the treatment volume.
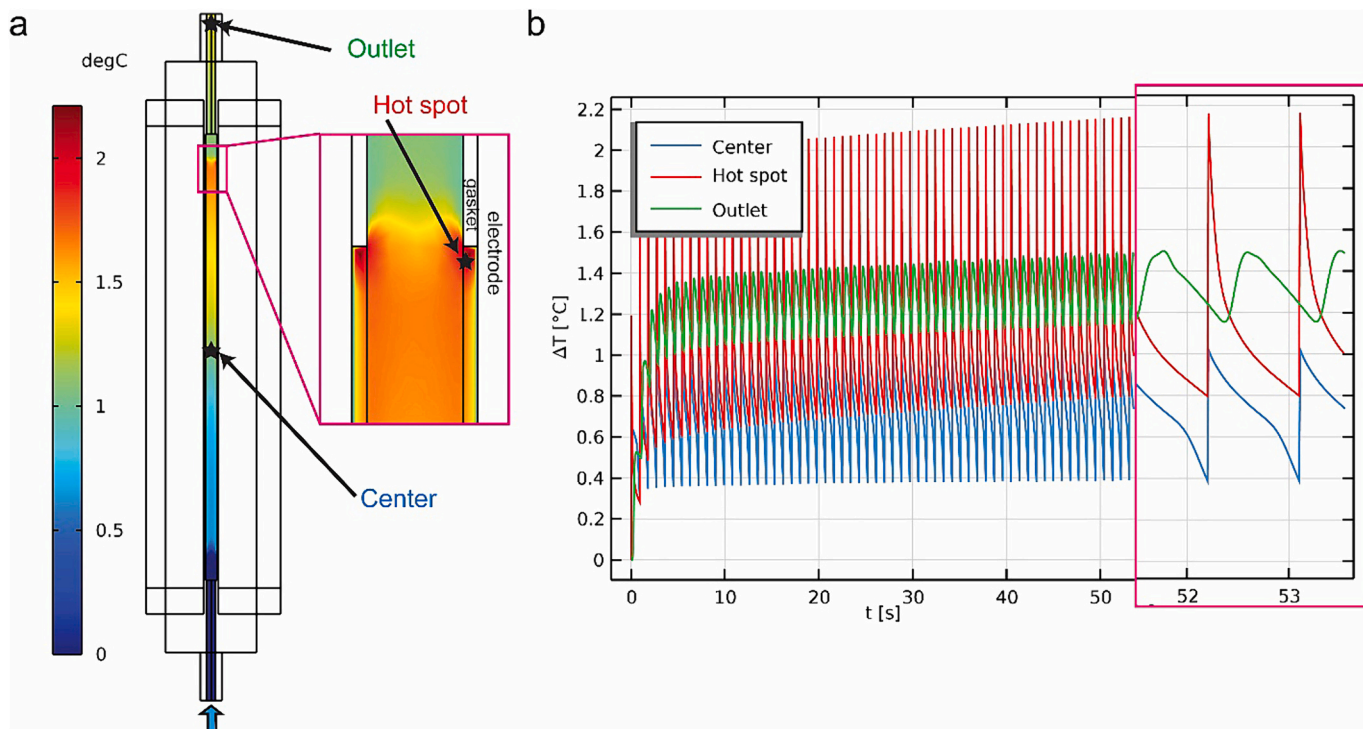

Fig. 7. (a) Simulated temperature distribution along the longitudinal symmetry plane (through the electrodes) of the parallel plate treatment chamber at the end of last simulated pulse for pulse protocol: continuous 100 μs, 1 Hz, U = 1000 V and F = 20 ml/min. (b) Temperature change evaluated at three different locations in the chamber (Hot spot, Outlet, Center - visible in (a)), for the same pulse protocol.

3.3. Comparison: time-dependent vs "duty cycle" approach to modelling of the electric field and heating

To compare the time-dependent modelling approach to the duty cycle approach, first the continuous 100 μs, 1 Hz PEF protocol used in experiments (Table 1), was modelled for both treatment chambers with the time-dependant approach (described in Section 2.3) and the duty cycle approach (described in the Introduction). To ensure exactly the same energy input for both modelling approaches, we used idealized square-shaped pulses (instead of a representative pulse from the voltage recording) with a rise and fall time of 0.1 μs in the time-dependent model. For the duty cycle approach the same finite element mesh, output times, solver configurations, physics and boundary conditions were used as described in Section 2.3, the only difference compared to the time-dependent approach was the use of time-invariant voltage as a boundary condition for the active electrode and multiplication of (now) steady state ohmic heating source (Q) by the duty factor (τf).

Simulation times for the duty cycle approach were approximately three times shorter than for the time-dependent approach for both treatment chambers. However, in case of duty cycle approach, the simulation times can be further shortened by increasing the time step size in the time-dependent study without losing any relevant information.

Fig. 8 shows the comparison of temperatures evaluated at the three different locations for both treatment chambers and modelling approaches.

Fig. 8 shows that the duty cycle approach for both treatment chambers provides a good representation of the average temperatures at different locations in the chamber. However, it smooths out the transient variations in temperature that occur during and in between electrical pulses, i.e. we lose the information on the peak temperature at the end of the pulse, and the decrease in temperature in between pulses. In the case of outlet temperature in colinear treatment chamber, where temperature oscillations are not present due to the large distance from the treatment volume, both modelling approaches predict comparable amplitude and the temporal dynamics of the temperature rise.

Even though the temperature oscillations visible in the Fig. 8 can be considered large in the relative sense (i.e. compared to the total temperature rise), they are small in the absolute sense ($< 1\ °C$). So, in the case of these PEF protocols and treatment chambers, predicting the temperature with duty cycle approach could be considered sufficient/ reasonable (subject to the demands of the application of course). However, the continuous 100 μs, 1 Hz PEF protocol used in the comparison employs relatively low fluid flows, electric fields (VDR < 3 kV/cm), and total specific energy inputs (WT under 8 kJ/kg), which is not representative of the PEF protocols used on the industrial scale. In the industrial use of PEF, protocols with much higher energies, fluid flows, and electric fields are used, which often result in large temperature increases in the treated product. For this reason, we believe it is important to also explore the potential difference between both modelling approaches for the "higher energy" PEF protocols.

3.4. Exploring the difference between modelling approaches for a hypothetical, "higher energy" PEF protocol

To further explore and demonstrate the difference between both modelling approaches, we decided to calculate the temperature in the colinear treatment chamber for a hypothetical "higher energy" PEF protocol: continuous 100 μs, 1 Hz, $U = 14,000$ V, and flow rate ($F = 2\ 1/$ h). These PEF parameters results in a *VDR* of 10 kV/cm and total specific energy input of $W_T \approx 71\ kJ/kg$, which is closer to the electric fields and energies used on the industrial scale. Results of comparison of the
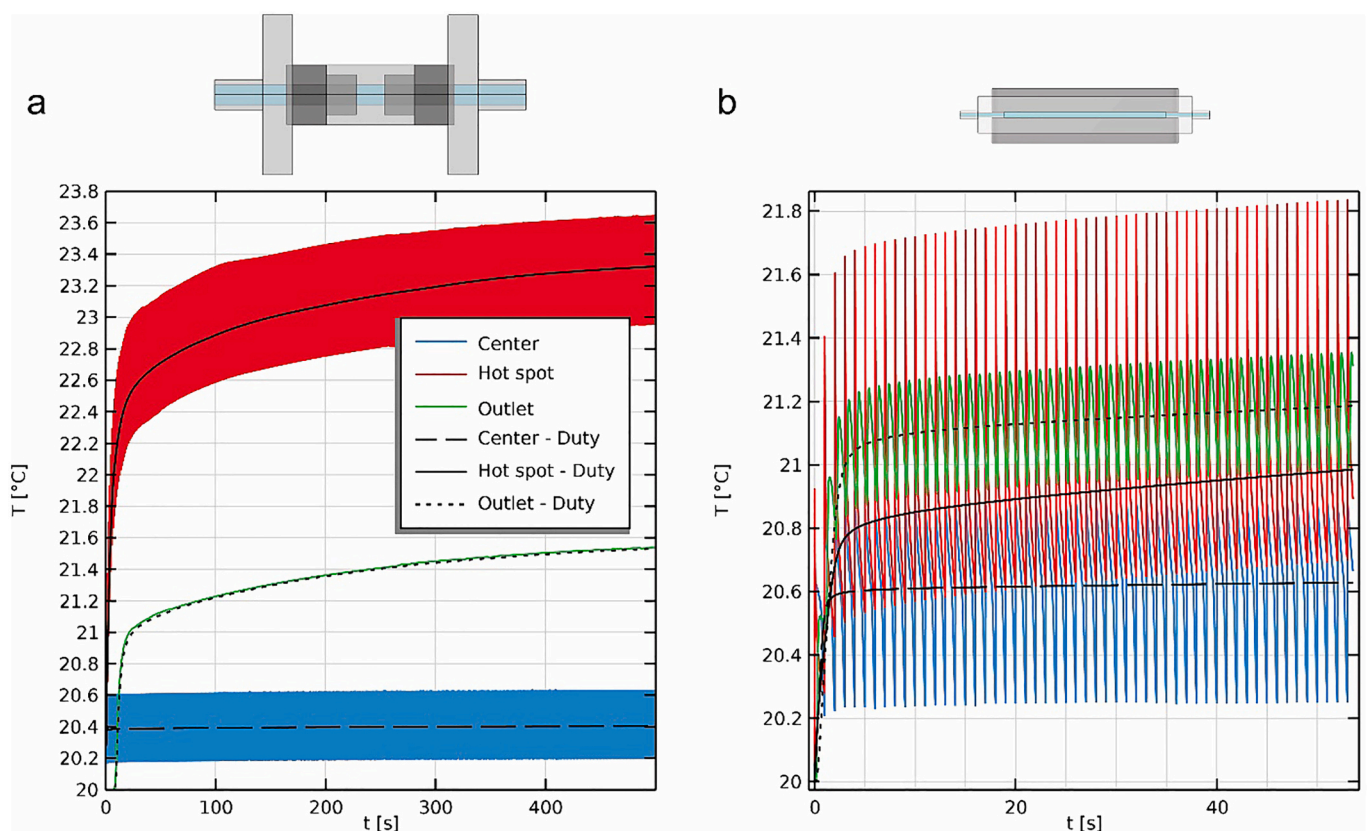

Fig. 8. Comparison of time-dependent model vs. duty cycle model. Temperatures evaluated at the three different locations in the (a) colinear and (b) parallel plate treatment chamber (Hot spot, Outlet, Center - visible in Fig. 6a and Fig. 7a). Pulse protocol: continuous 100 μs, 1 Hz, $F = 20$ ml/min, T_i=20 °C and $U = 1000$ V (parallel plate) and $U = 4000$ V (colinear). Evaluated temperatures corresponding to the duty cycle model are denoted by "- Duty" in the legend.

modelling approaches are shown in Fig. 9.

We would like to note that due to equipment limitations (syringe pump, pulse generator) we did not perform model validation for the higher energy PEF protocol, so the modelling study presented in this subsection should be understood as purely an in silico-study. However, even though this protocol falls outside the range of PEF parameters within which we validated our model, we believe the results of the calculations can still be considered reasonably accurate, since the physics and boundary conditions used in the validated model (described in Section 2.3) are still applicable; flow can be still be considered laminar ($Re = 71$), calculated temperatures in the treatment volume are within the range of the temperature-dependent electrical conductivity model of the saline solution, and pulse protocol with the same pulse width and frequency as validated in our study was used. We have also checked the validity of thermal insulation boundary condition at the treatment chamber surface, i.e., we tested if natural convection affects the temperature in the fluid volume, and simulation results showed its contribution to be negligible, at least for the observed simulation times.

Fig. 9 shows that in this specific demonstrated case of higher energy PEF protocol, the time-dependent approach shows large temperature fluctuations (over 10 °C peak-to-peak difference), which are not accounted for with the duty cycle approach. This is notable especially in the hot spot where the time-dependent model predicts peak temperatures around 70 °C, compared to duty cycle model that anticipates around 62 °C (Fig. 9c). This 8 °C difference might not seem like a lot, however, depending on the application, it may be unacceptable.

Fig. 9 also shows that at the outlet of the colinear treatment chamber duty cycle approach predicts a lower temperature compared to the time-dependent approach. This discrepancy also points to potential underestimation of temperature in the treatment chamber by the duty cycle approach or overestimation of the temperature by the time-dependent approach. It is also important to note that this discrepancy between the modelling approaches is a function of both the PEF protocol and treatment chamber geometry and should thus be further explored and validated.

For a full evaluation of the difference between the time-dependent and duty cycle modelling approach, a more comprehensive study would need to test different edge cases of PEF protocols and geometries,

preferably more relevant to the industrial use of PEF, however, such a study is beyond the scope of this paper. Moreover, it needs to be emphasized that the model would first need to be thoroughly validated for these higher energy, higher flow rates PEF protocols. To gain further confidence in the model it would also be important to somehow measure the temperatures at the hot spots, where the model shows the highest temperature rise and largest temperature fluctuations. The purpose of the results shown herein is only to illustrate the possibilities and advantages of the more temporally-precise modelling approach and point to the potential differences in both modelling approaches.

4. Conclusions

The presented time-dependent model of temperature distribution in continuous flow PEF treatment chamber shows a good agreement with the experimentally measured electric current and temperature for both treatment chambers and different PEF protocols, indicating a successful validation of the model and showing the potential to use the model independent of the pulse protocol, flow parameters, and treatment chamber design (geometry, etc.).

The new modelling approach simulates each electrical pulse separately by using either the experimentally measured voltage waveform or ideal square-shaped pulses. This allows for an analysis of the electrical current, electric field, and temperature distribution in the chamber during, at the end, and in between application of electrical pulses. The use of experimentally measured voltage in the model enables us the possibility to accurately model also more irregularly shaped electrical pulses with longer rise and fall times.

The time-dependent modelling approach gives us insight into temperature fluctuations at different spatial locations in the chamber caused by delivery of pulsed field energy, which are not accounted for in the "duty cycle" approach. These temperature fluctuations can be considered noteworthy, depending on the PEF protocol. If the temperature fluctuations in the hot spots are large enough, the duty cycle model might fail to predict the potential thermal damage to the product traveling through the treatment volume, or in extreme cases even potential local boiling of the medium, resulting not only in degradation of the treated material, but also in accelerated electrode fouling, oxidation,
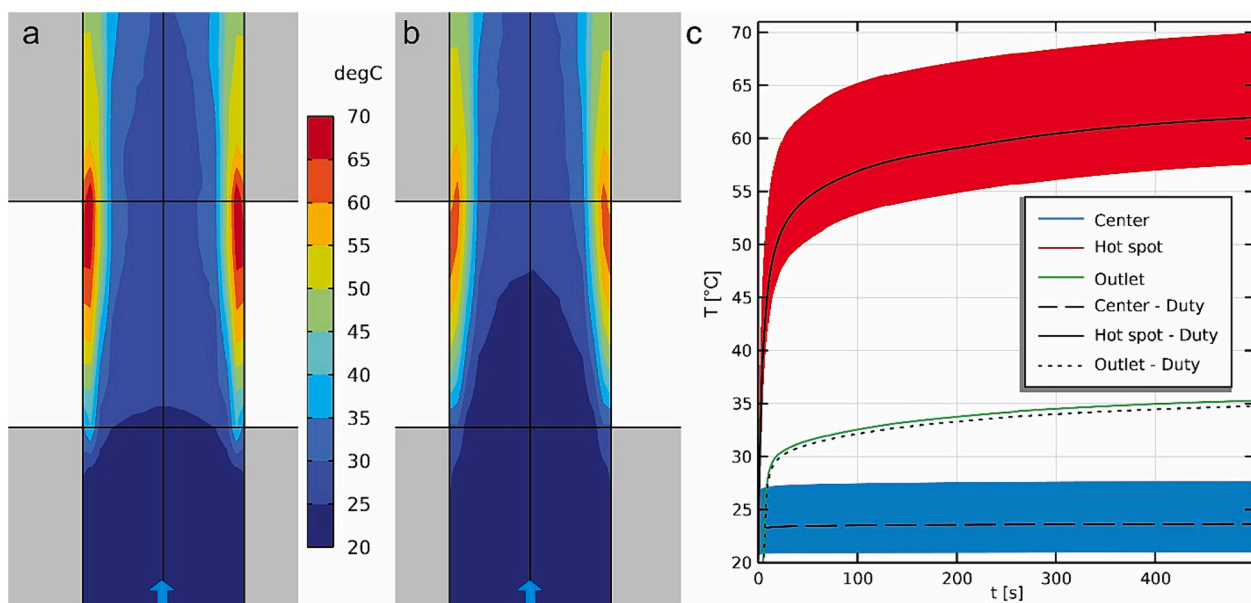

Fig. 9. Comparison of time-dependent model vs. duty cycle model. On the left, simulated spatial temperature distribution of the colinear treatment chamber at the last simulated pulse for pulse protocol: continuous 100 μs, 1 Hz, $U = 14,000$ V, T_i=20 °C and $F = 2$ l/h for the time-dependent model a) and for the duty cycle model b). On the right, comparison of temperatures evaluated at the three different locations in the colinear chamber (visible in Fig. 6a) for both modelling approaches (c). Evaluated temperatures corresponding to the duty cycle model are denoted by "- Duty" in the legend.

and dissolution (etching), as well as arcing (Morren, Roodenburg, & de Haan, 2003). This would not only affect the quality of the treated product but would also affect the wear and lifetime of electrodes/ chambers, and of the pulse generator. The time-dependent modelling approach thus opens the possibility of more accurate estimation of over/ under treatment.

Since our modelling approach allows for the analysis of temporally variable temperature and electric field distribution in the treatment chamber, it also potentially enables to look at the exposure of a single particle/cell within the treated product to temperature and electric field strength as it moves through the treatment chamber based on its trajectory.

The limitation of the time-dependent modelling approach is the computational intensity of the model, which results in long simulations times compared to the duty cycle approach. This can become problematic if we are interested in reaching the stationary state in simulations for which many pulses would be needed, or in case of more complex treatment chamber geometries or large parametric studies.

CRediT authorship contribution statement

Peter Lombergar: Writing – original draft, Visualization, Methodology, Investigation, Formal analysis. **Karel Flisar:** Writing – review & editing, Investigation. **Damijan Miklavčič:** Writing – review & editing, Supervision, Conceptualization. **Samo Mahnič-Kalamiza:** Writing – review & editing, Writing – original draft, Supervision, Methodology, Conceptualization.

Declaration of competing interest

The authors declare that they have no known competing financial interests or personal relationships that could have appeared to influence the work reported in this paper.

Data availability

Data will be made available on request.

Acknowledgements

Appendix A. Supplementary data

Supplementary data to this article can be found online at https://doi.org/10.1016/j.ifset.2024.103628.

References

Ballash, G. A., Lee, S., Mollenkopf, D. F., Mathys, D. A., Albers, A. L., Sechrist, E., … Wittum, T. E. (2020). Pulsed electric field application reduces carbapenem- and colistin-resistant microbiota and blaKPC spread in urban wastewater. *Journal of Environmental Management, 265*, Article 110529. https://doi.org/10.1016/j.jenvman.2020.110529

Bermúdez-Aguirre, D., Dunne, C. P., & Barbosa-Cánovas, G. V. (2012). Effect of processing parameters on inactivation of Bacillus cereus spores in milk using pulsed electric fields. *International Dairy Journal, 24*(1), 13–21. https://doi.org/10.1016/j.idairyj.2011.11.003

Buckow, R., Schroeder, S., Berres, P., Baumann, P., & Knoerzer, K. (2010). Simulation and evaluation of pilot-scale pulsed electric field (PEF) processing. *Journal of Food Engineering, 101*(1), 67–77. https://doi.org/10.1016/j.jfoodeng.2010.06.010

Buckow, R., Semrau, J., Sui, Q., Wan, J., & Knoerzer, K. (2012). Numerical evaluation of lactoperoxidase inactivation during continuous pulsed electric field processing. *Biotechnology Progress, 28*(5), 1363–1375. https://doi.org/10.1002/btpr.1582

Delso, C., Berzosa, A., Sanz, J., Álvarez, I., & Raso, J. (2021). Microbial decontamination by pulsed electric fields (PEF) in winemaking. In *Grapes and wine [working title]*. IntechOpen. https://doi.org/10.5772/intechopen.101112

Eleršek, T., Flisar, K., Likozar, B., Klemenčič, M., Golob, J., Kotnik, T., & Miklavčič, D. (2020). Electroporation as a solvent-free green technique for non-destructive extraction of proteins and lipids from Chlorella vulgaris. *Frontiers in Bioengineering and Biotechnology, 8*, 443. https://doi.org/10.3389/fbioe.2020.00443

Fiala, A., Wouters, P. C., van den Bosch, E., & Creyghton, Y. L. M. (2001). Coupled electrical-fluid model of pulsed electric field treatment in a model food system. *Innovative Food Science & Emerging Technologies, 2*(4), 229–238. https://doi.org/10.1016/S1466-8564(01)00042-X

Flisar, K., Meglic, S. H., Morelj, J., Golob, J., & Miklavcic, D. (2014). Testing a prototype pulse generator for a continuous flow system and its use for E. Coli inactivation and microalgae lipid extraction. *Bioelectrochemistry, 100*, 44–51. https://doi.org/10.1016/j.bioelechem.2014.03.008

Gabrić, D., Barba, F., Roohinejad, S., Gharibzahedi, S. M. T., Radojčin, M., Putnik, P., & Bursać Kovačević, D. (2018). Pulsed electric fields as an alternative to thermal processing for preservation of nutritive and physicochemical properties of beverages: A review. *Journal of Food Process Engineering, 41*(1), Article e12638. https://doi.org/10.1111/jfpe.12638

Geboers, B., Scheffer, H. J., Graybill, P. M., Ruarus, A. H., Nieuwenhuizen, S., Puijk, R. S., … Meijerink, M. R. (2020). High-voltage electrical pulses in oncology: Irreversible electroporation, electrochemotherapy, gene electrotransfer, electrofusion, and electroimmunotherapy. *Radiology, 295*(2), 254–272. https://doi.org/10.1148/radiol.2020192190

Gerlach, D., Alleborn, N., Baars, A., Delgado, A., Moritz, J., & Knorr, D. (2008). Numerical simulations of pulsed electric fields for food preservation: A review. *Innovative Food Science & Emerging Technologies, 9*(4), 408–417. https://doi.org/10.1016/j.ifset.2008.02.001

Golberg, A., Sack, M., Teissie, J., Pataro, G., Pliquett, U., Saulis, G., Stefan, T., Miklavcic, D., Vorobiev, E., & Frey, W. (2016). Energy-efficient biomass processing with pulsed electric fields for bioeconomy and sustainable development. *Biotechnology for Biofuels, 9*(1), 94. https://doi.org/10.1186/s13068-016-0508-z

Góngora-Nieto, M. M., Pedrow, P. D., Swanson, B. G., & Barbosa-Cánovas, G. V. (2003). Impact of air bubbles in a dielectric liquid when subjected to high field strengths. *Innovative Food Science & Emerging Technologies, 4*(1), 57–67. https://doi.org/10.1016/S1466-8564(02)00067-X

Harris, E., & Elmer, J. J. (2021). Optimization of electroporation and other non-viral gene delivery strategies for T cells. *Biotechnology Progress, 37*(1), Article e3066. https://doi.org/10.1002/btpr.3066

Huang, K., Yu, L., Gai, L., & Wang, J. (2013). Coupled simulations in colinear and coaxial continuous pulsed electric field treatment chambers. *Transactions of the ASABE, 1473–1484*. https://doi.org/10.13031/trans.56.9167

Jaeger, H., Meneses, N., & Knorr, D. (2009). Impact of PEF treatment inhomogeneity such as electric field distribution, flow characteristics and temperature effects on the inactivation of E. coli and milk alkaline phosphatase. *Innovative Food Science & Emerging Technologies, 10*(4), 470–480. https://doi.org/10.1016/j.ifset.2009.03.001

Knoerzer, K., Baumann, P., & Buckow, R. (2012). An iterative modelling approach for improving the performance of a pulsed electric field (PEF) treatment chamber. *Computers & Chemical Engineering, 37*, 48–63. https://doi.org/10.1016/j.compchemeng.2011.09.002

Kotnik, T., Frey, W., Sack, M., Haberl Meglič, S., Peterka, M., & Miklavčič, D. (2015). Electroporation-based applications in biotechnology. *Trends in Biotechnology, 33*(8), 480–488. https://doi.org/10.1016/j.tibtech.2015.06.002

Kotnik, T., Kramar, P., Pucihar, G., Miklavcic, D., & Tarek, M. (2012). Cell membrane electroporation- part 1: The phenomenon. *IEEE Electrical Insulation Magazine, 28*(5), 14–23. https://doi.org/10.1109/MEI.2012.6268438

Kotnik, T., Rems, L., Tarek, M., & Miklavčič, D. (2019). Membrane electroporation and Electropermeabilization: Mechanisms and models. *Annual Review of Biophysics, 48*(1), 63–91. https://doi.org/10.1146/annurev-biophys-052118-115451

Lindgren, M., Aronsson, K., Galt, S., & Ohlsson, T. (2002). Simulation of the temperature increase in pulsed electric field (PEF) continuous flow treatment chambers. *Innovative Food Science & Emerging Technologies, 3*(3), 233–245. https://doi.org/10.1016/S1466-8564(02)00044-9

Mahnič-Kalamiza, S., Vorobiev, E., & Miklavčič, D. (2014). Electroporation in food processing and biorefinery. *The Journal of Membrane Biology, 247*(12), 1279–1304. https://doi.org/10.1007/s00232-014-9737-x

Mañas, P., & Pagán, R. (2005). Microbial inactivation by new technologies of food preservation. *Journal of Applied Microbiology, 98*(6), 1387–1399. https://doi.org/10.1111/j.1365-2672.2005.02561.x

McCleskey, R. B. (2011). Electrical conductivity of electrolytes found in natural waters from (5 to 90) °C. *Journal of Chemical & Engineering Data, 56*(2), 317–327. https://doi.org/10.1021/je101012n

Meneses, N., Jaeger, H., Moritz, J., & Knorr, D. (2011). Impact of insulator shape, flow rate and electrical parameters on inactivation of E. coli using a continuous co-linear PEF system. *Innovative Food Science & Emerging Technologies, 12*(1), 6–12. https://doi.org/10.1016/j.ifset.2010.11.007

Morales-de la Peña, M., Elez-Martínez, P., & Martín-Belloso, O. (2011). Food preservation by pulsed electric fields: An engineering perspective. *Food Engineering Reviews, 3*(2), 94–107. https://doi.org/10.1007/s12393-011-9035-7

Morren, J., Roodenburg, B., & de Haan, S. W. H. (2003). Electrochemical reactions and electrode corrosion in pulsed electric field (PEF) treatment chambers. *Innovative Food*

Science & Emerging Technologies, 4(3), 285–295. https://doi.org/10.1016/S1466-8564(03)00041-9

Pataro, G., Ferrentino, G., Ricciardi, C., & Ferrari, G. (2010). Pulsed electric fields assisted microbial inactivation of S. cerevisiae cells by high pressure carbon dioxide. *The Journal of Supercritical Fluids, 54*(1), 120–128. https://doi.org/10.1016/j.supflu.2010.04.003

Prasad Lamsal, B., & Kumar Jindal, V. (2014). Variation in electrical conductivity of selected fruit juices during continuous Ohmic heating. *KMUTNB International Journal of Applied Science and Technology, 7*(1), 47–56. https://doi.org/10.14416/j.ijast.2014.01.008

Qin, B., Zhang, Q., Barbosa-Cánovas, G. V., Swanson, B. G., & Pedrow, P. D. (1995). Pulsed electric field treatment chamber design for liquid food pasteurization using a finite element method. *Transactions of ASAE, 38*(2), 557–565. https://doi.org/10.13031/2013.27866

Raso, J., Frey, W., Ferrari, G., Pataro, G., Knorr, D., Teissie, J., & Miklavčič, D. (2016). Recommendations guidelines on the key information to be reported in studies of application of PEF technology in food and biotechnological processes. *Innovative Food Science & Emerging Technologies, 37*, 312–321. https://doi.org/10.1016/j.ifset.2016.08.003

Rebersek, M., Miklavcic, D., Bertacchini, C., & Sack, M. (2014). Cell membrane electroporation-part 3: The equipment. *IEEE Electrical Insulation Magazine, 30*(3), 8–18. https://doi.org/10.1109/MEI.2014.6804737

Rems, L., & Miklavčič, D. (2016). Tutorial: Electroporation of cells in complex materials and tissue. *Journal of Applied Physics, 119*(20), Article 201101. https://doi.org/10.1063/1.4949264

Sachdev, S., Potočnik, T., Rems, L., & Miklavčič, D. (2022). Revisiting the role of pulsed electric fields in overcoming the barriers to in vivo gene electrotransfer.

Bioelectrochemistry, 144, Article 107994. https://doi.org/10.1016/j.bioelechem.2021.107994

Schottroff, F., Knappert, J., Eppmann, P., Krottenthaler, A., Horneber, T., McHardy, C., … Jaeger, H. (2020). Development of a continuous pulsed electric field (PEF) vortex-flow chamber for improved treatment homogeneity based on hydrodynamic optimization. *Frontiers in Bioengineering and Biotechnology, 8*, 340. https://doi.org/10.3389/fbioe.2020.00340

Toepfl, S., Heinz, V., & Knorr, D. (2007). High intensity pulsed electric fields applied for food preservation. *Chemical Engineering and Processing: Process Intensification, 46*(6), 537–546. https://doi.org/10.1016/j.cep.2006.07.011

Toepfl, S., Mathys, A., Heinz, V., & Knorr, D. (2006). Review: Potential of high hydrostatic pressure and pulsed electric fields for energy efficient and environmentally friendly food processing. *Food Reviews International, 22*(4), 405–423. https://doi.org/10.1080/87559120600865164

Toepfl, S., Siemer, C., Saldaña-Navarro, G., & Heinz, V. (2014). Overview of pulsed electric fields processing for food. In *Emerging Technologies for Food Processing* (pp. 93–114). Elsevier. https://doi.org/10.1016/B978-0-12-411479-1.00006-1.

Verma, A., Asivatham, S. J., Deneke, T., Castellvi, Q., & Neal, R. E. (2021). Primer on pulsed electrical field ablation: Understanding the benefits and limitations. *Circulation: Arrhythmia and Electrophysiology, 14*(9). https://doi.org/10.1161/CIRCEP.121.010086

Yarmush, M. L., Golberg, A., Serša, G., Kotnik, T., & Miklavčič, D. (2014). Electroporation-based Technologies for Medicine: Principles, applications, and challenges. *Annual Review of Biomedical Engineering, 16*(1), 295–320. https://doi.org/10.1146/annurev-bioeng-071813-104622